Atomistic simulation of damage production by atomic and molecular ion irradiation in GaN

M. W. Ullah, A. Kuronen, K. Nordlund, F. Djurabekova, P. A. Karaseov et al.

Citation: J. Appl. Phys. **112**, 043517 (2012); doi: 10.1063/1.4747917
View online: http://dx.doi.org/10.1063/1.4747917
View Table of Contents: http://jap.aip.org/resource/1/JAPIAU/v112/i4
Published by the American Institute of Physics.

Atomistic simulation of damage production by atomic and molecular ion irradiation in GaN

M. W. Ullah,[1,a)] A. Kuronen,[1] K. Nordlund,[1] F. Djurabekova,[1] P. A. Karaseov,[2] and A. I. Titov[2]
[1]*Department of Physics, University of Helsinki, P.O. Box 64, FIN-00014 Helsinki, Finland*
[2]*St. Petersburg State Polytechnic University, 195251 St. Petersburg, Russia*

(Received 16 March 2012; accepted 20 July 2012; published online 30 August 2012)

We have studied defect production during single atomic and molecular ion irradiation having an energy of 50 eV/amu in GaN by molecular dynamics simulations. Enhanced defect recombination is found in GaN, in accordance with experimental data. Instantaneous damage shows non-linearity with different molecular projectile and increasing molecular mass. Number of instantaneous defects produced by the PF_4 molecule close to target surface is four times higher than that for PF_2 molecule and three times higher than that calculated as a sum of the damage produced by one P and four F ion irradiation ($P + 4 \times F$). We explain this non-linearity by energy spike due to molecular effects. On the contrary, final damage created by PF_4 and PF_2 shows a linear pattern when the sample cools down. Total numbers of defects produced by Ag and PF_4 having similar atomic masses are comparable. However, defect-depth distributions produced by these species are quite different, also indicating molecular effect. © *2012 American Institute of Physics*. [http://dx.doi.org/10.1063/1.4747917]

I. INTRODUCTION

The past decade has seen dramatic advances in the development of wide band gap semiconductors, such as GaN in devices ranging from blue lasers to solar cells.[1,2] Apart from the light emitting devices which typically require long carrier lifetimes, another class of components based on short lifetimes is being developed. Nowadays, terahertz technology has many promising applications in medical, biological and industrial imaging, safety communication, space science, etc. GaN, a wide band gap semiconductor with inherently high breakdown field (3.5×10^6 V/m), high electron saturation velocity (2 MV/cm), and high thermal conductivity (1.3 W/cm K), possesses large potential to reach high power of terahertz radiation.[3]

Ion implantation is a central part of modern semiconductor processing, as it is used to introduce electrically and optically active dopants into materials. In particular, ion implantation can be used for electrical compensation and tuning of carrier lifetime. It offers wide possibilities of defect engineering through the choice of implantation species, dose, and energy. Compensation is achieved by introducing damage-related deep levels that capture free carriers. Moreover, it has recently become clear that ion irradiation can also be used to speed up the operation of semiconductor lasers by up to 2 orders of magnitude.[4,5] A result of particular interest obtained from studies of this effect was that heavy ion irradiation is more efficient at producing this effect than light ions.[6] The choice of ions depends on thickness of the semiconductor layer and on desired kind of defects. For example, implantation of low mass ions, such as protons, produces only point defects through the traversed layer; only at the depth of the stopping range, extended defects may occur. On the other hand, high mass ions, such as Ga or Xe, produce damage in clusters and can thus affect the optical properties in a very different manner. As a further extension of this idea, molecular and nanocluster ions can produce even larger defect clusters. Thus, ion and cluster ion implantation can produce a wide variety of different kinds of material modification. While the effects of single ion irradiation on optical properties of materials have been explored widely, cluster ion irradiation has barely been studied.

Our previous experiments have, however, shown that at 1.3 keV/amu energy, the damage production itself in GaN is non-linear with molecule size.[7–10] This gives a strong motivation for theoretical studies of the molecular effects.

In this work, we focus on the details of molecular irradiation process in order to gain a clear understanding of the inherent differences of single atomic ion and molecular ion irradiation, also compare irradiation effects in GaN by molecular dynamics (MD) simulations. Of particular interest is, whether the damage increases non-linearly with the number of atoms in a molecule, as previously reported for some cases of cluster ion irradiation of metals.[11,12] Several projectiles, such as F, P, Ar, Ag, PF_2, and PF_4, have been used for irradiation.

II. METHOD

The interaction between atoms in GaN was described using a Tersoff-like many body interatomic potential previously developed in our group.[13] The cohesion of PF_2 and PF_4 molecules was modeled using the Lennard-Jones potential ($V(r) = 4\epsilon[(\sigma/r)^{12} - (\sigma/r)^6]$) in such a way that it describes correctly bond lengths, bond energies, and bond angles of the molecules (see Table I, Figure 1). Dissociation energies (ϵ) were chosen as 4.6 and 1.6585 eV (Refs. 14–16)

a)Electronic mail: mohammad.ullah@helsinki.fi.

TABLE I. Values of geometrical parameters of PF_2 and PF_4 molecules (see Figure 1) used in simulation and compared with experimental and theoretical results.[14–16] Bond lengths are in Å and bond angles in degrees.

Geometrical parameters			
Molecule	Parameters	Simulation	Reference
PF_2	ℓ	1.579	1.579
	θ	98.83	98.5
PF_4	ℓ_1	1.54	1.54
	ℓ_2	1.59	1.61
	θ_1	105.09	103.7
	θ_2	166.41	164.6

and the bond length parameters (σ) were determined as 1.408 and 2.131 Å for the P–F and F–F bonds, respectively. The Ziegler-Biersack-Littmark (ZBL) universal repulsive potential[17] was smoothly joined to all these potentials to describe the interaction at high energies. The electronic stopping was applied as a friction force for atoms with kinetic energies higher than 1 eV and calculated using the SRIM version 2008.04 (Ref. 18).

An adaptive time step MD code PARCAS[19] was used for the simulations. The GaN simulation cells were created using the wurtzite (WZ) crystal structure with an orthogonal unit cell corresponding to two conventional hexagonal unit cells. The simulation cell contained 120 000 atoms and had the size of $111 \times 110 \times 109$ Å^3. The simulation cell was relaxed at 300 K before irradiation. Irradiations were performed on the (0001) surface of the WZ structure, where the boundary condition was open. Periodic boundary conditions were applied in the lateral directions. The bottom of the simulation cell was fixed to avoid drifting. Twenty irradiations were done by each type of projectile on a pristine sample to collect statistics. Energies for F, P, Ar, Ag, PF_2, and PF_4 projectiles were 0.95, 1.55, 2, 5.35, 3.45, and 5.35 keV, respectively. The energies were chosen in such a way that energy/atomic-mass was the same (0.05 keV/amu) for all atoms and molecules. The atomic ion and molecular ion projectiles were placed above the simulation cell surface and to avoid channelling, the bombardments were done with 7° angle off the *c*-axis. Impact points were chosen randomly, i.e., for each impact, a virgin sample was taken and the atoms in the simulation cell were shifted by a random distance in the *x* and *y* directions, then a new irradiation was performed.

Berendsen temperature control[20] was used on the periodic boundaries of the simulation cell to remove excess heat produced by the cascades. No pressure control was used as there was a free surface in the system.

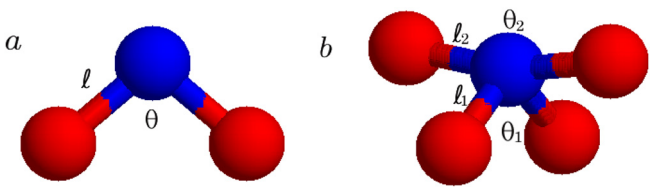

FIG. 1. Geometries of a) PF_2 and b) PF_4 molecules.

Defect analysis was done by Voronoi-polyhedron approach by comparing irradiated and pristine lattices. Polyhedra with no atoms were labeled vacancies, polyhedra with two or more atoms interstitials, and polyhedra with one atom of the opposite type to the initial one antisites.[21,22]

III. RESULTS AND DISCUSSION

In Figure 2(a), time dependence of the average number of vacancies per projectile for all ions is presented. It clearly shows that even though GaN is a semiconductor, there is a fairly strong in-cascade damage recombination in the material. The damage peak at about 0.25 ps is roughly 10 times higher for PF_4 and Ag, and 7 times higher for PF_2 than the final damage after the cascade has cooled down. This recombination value ($\sim$10) is much less than in metals; for instance in Fe typical values are $\sim$50 (Ref. 23). On the other hand, it is still somewhat more pronounced than in Si, where the recombination is only a factor of 2-3 (Ref. 21). There is also a second peak around 2 ps of PF_4 and Ag irradiation. By the visual inspection of the simulations system, it was observed that the peaks result from the elastic waves caused by the collapse of the cascade region. By doing a simulation with a box nine times larger and still seeing the peak at the same time ascertained that the second peak is not a finite size effect. It should be noted that such elastic vibrations can influence also the number of instantaneous defects.

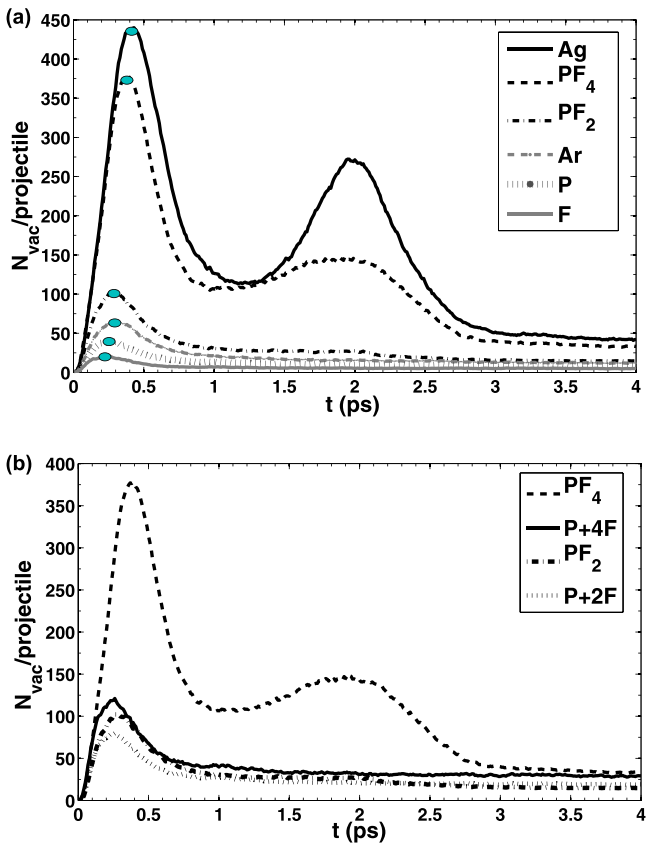

FIG. 2. (a) Time development of the number of defects. The curves are averages of twenty irradiations. The ellipsoidal dots show the time step having the highest number of vacancies which corresponds to non-linearity proposed in Figures 4 and 5. (b) Time development of the number of defects of molecular projectiles compared with those calculated as corresponding to linear combinations of single ion irradiations (P + 4 × F and P + 2 × F).

TABLE II. Average number of defects and sputtered atoms produced by different projectiles after irradiation with a single ion. Uncertainties are the statistical errors of sets of 20 irradiations.

Projectile type	Energy (keV)	Vacancies	Interstitials	Antisites	Sputtered
F	0.95	5 ± 1	5 ± 1	4 ± 1	1
P	1.55	9 ± 2	8 ± 1	8 ± 1	1
Ar	2	11 ± 2	10 ± 1	10 ± 1	2
PF_2	3.45	14 ± 1	16 ± 1	17 ± 1	4
PF_4	5.35	29 ± 3	28 ± 2	32 ± 3	7
Ag	5.35	37 ± 5	32 ± 3	33 ± 3	2

Figure 2(b) shows – along with the number of vacancies produced by the molecular projectiles – number of vacancies calculated as linear combinations $N_{vac}(P) + 2N_{vac}(F)$ and $N_{vac}(P) + 4N_{vac}(F)$. Without any molecular effects causing non-linearities in defect production, these curves should coincide with the corresponding molecular irradiation curves. For PF_2, this is more or less the case. However, in the case of PF_4, the amount of damage by the molecular projectile is 2–3 times higher than that of the linear combination of single ion damages at times less than 2.5 ps. After that the curves coincide. Final number of defects shown in Table II corroborates this linear behavior.

The reason for the observed appearance of linearity in the case of PF_4 is probably the enhanced recombination of damage caused by the dense cascade of a heavy molecule. This leads to the fact that at the used ion energy, final defect production between the atomic ion and molecular ion irradiation does not exhibit a notable difference. However, we have clearly observed such a difference experimentally at higher energies. Therefore, further investigation on the threshold irradiation energy by means of atomistic simulation at which this difference becomes significant is required for the practical applications.

A visual comparison of defect production by different projectiles is shown in Figure 3. It clearly shows, with increasing atomic and molecular mass number of defects increases.

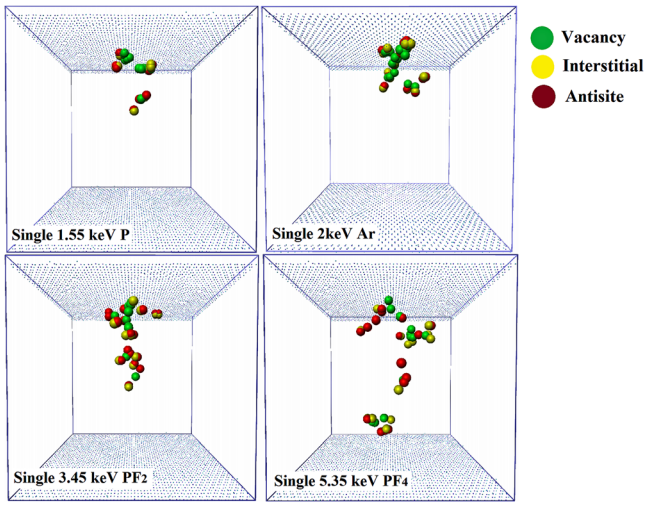

FIG. 3. Snapshots of defects produced with different projectiles. Only defects are shown in the simulation cell. Vacancies, interstitials and antisites have been indicated by green, yellow and red color, respectively. These snapshots are taken at 20 ps.

Figure 4 shows the instantaneous defect (vacancy) depth distribution for all projectiles at the time step where the number of the defects is highest, i.e., when there is no defect recombination. It also shows depth distribution of final stage. The purpose of the plot is to compare MD with SRIM which does not take into account in-cascade defect recombination. It is seen that the lower the threshold displacement energy (E_d), the deeper and higher the maximum of nuclear energy

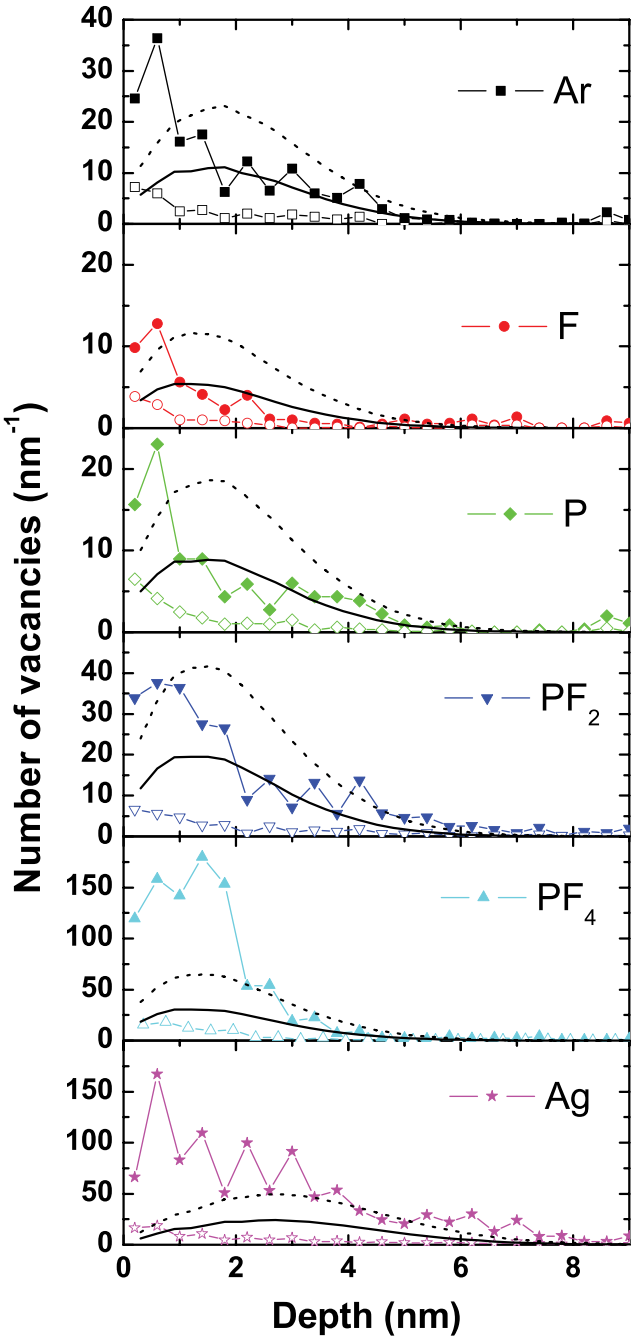

FIG. 4. Instantaneous (closed symbols) and final (open symbols) distribution of vacancies produced in GaN by different species together with SRIM[18] predicted vacancy distributions calculated using two different threshold displacement energies ED = 25 eV (solid line) and 12 eV (dot line). MD curves are calculated at the time of maximum defect number shown as ellipsoidal dots in Figure 2(a).

loss is. However, standard value of $E_d = 25$eV more or less describes the light mass generation. On the other hand, even twice lower E_d (12 eV) does not give us silver and PF_4 generation and twice overestimates light ion generation. High defect density is apparent close to the surface, and interestingly, the defect peak for PF_4 and Ag is four times higher than for PF_2. This indicates non-linear damage production with increasing molecular size. Also, by comparing molecular and heavy mass ion (Ag, PF_4 and PF_2) with single atomic ion (F, P, and Ar) irradiation, we can see that former ions produce significantly larger amount of lattice disorder close to the surface region. Thus, in Figure 4, contrary to the linearity seen in Table II, we observe a clear non-linear behaviour in instantaneous damage production. Another interesting feature is that for all atomic ions and molecular ions, MD calculated defects are closer to the surface than that calculated by SRIM.

We have done another kind of data analysis to give a better look at non-linear effect. Figure 5 shows defect depth distributions of molecular PF_4 and PF_2 projectiles in comparison with the corresponding linear combinations of single ion irradiations. It clearly demonstrates non-linear damage production in the case of PF_4. As we can see, the total number of defects close to surface is around three times higher for molecular projectile than for the combination of single ion irradiations. There can be very small non-linearities for PF_2 as the two curves practically coincide.

To explain the molecular effect, dissociation of the PF_4 molecule has been studied (Figure 6). One can see that at the beginning of the irradiation, molecules stay as a whole or atoms stay close to each other (interatomic distance less than $\sim 0.5 - 1$ nm). After that they start to dissociate but small interatomic distances are still observed. The fact that the atoms of the molecule stay near to each other till considerably large depths means that the damage distributions of individual atoms overlap giving rise to non-linear behavior of defect creation.

Thus, to summarize these observations, we find that at the peak damage time in the energy spike, there is a significant non-linear enhancement in the damage production for PF_4. However, the in-cascade dynamic annealing is quite strong (Figure 2), and in the end (Table II) there is no statistically

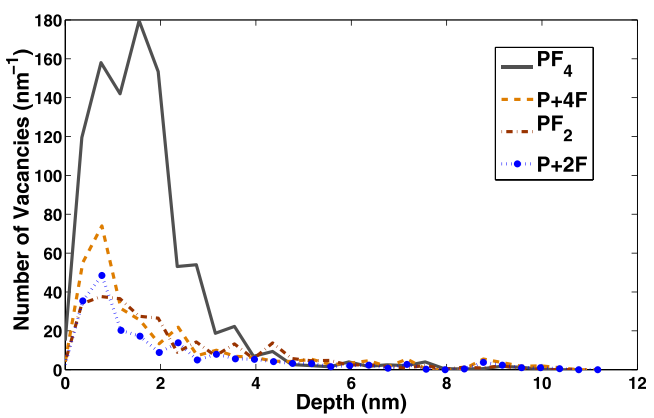

FIG. 5. Instantaneous depth distributions of defects produced by molecular projectiles. Also shown are the corresponding curves for linear combinations of single ion irradiations (P + 4 × F and P + 2 × F).

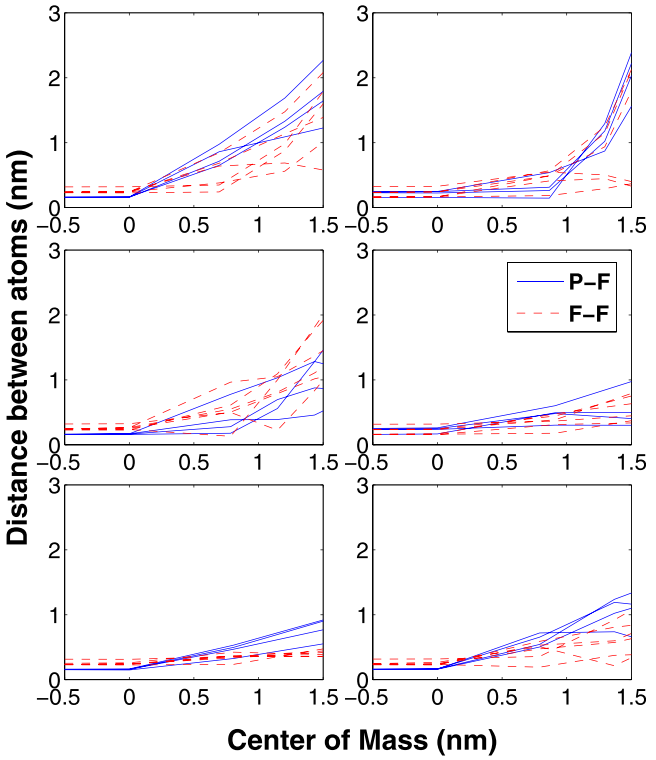

FIG. 6. Dissociation of the PF_4 molecule in irradiation simulations. Six different irradiation cases are shown. *x*-axis: center of mass of the molecule measured from the sample surface (zero of the axis), *y*-axis: interatomic distance between atoms.

significant enhancement of the final damage production. During prolonged irradiation, the non-linear enhancement of the heat spike could enhance damage production and amorphization by overlap with previous damage. This issue will be considered in future works by cascade overlap simulations.

IV. CONCLUSIONS

We have used molecular dynamics method to study damage production in GaN by ion irradiation. Both single atomic ions and molecular ions were used for irradiation. The results show indication of non-linear enhancement of instantaneous damage due to molecular effects and increasing mass of the projectile.

On the other hand, enhanced recombination of the damage due to dynamic annealing decreases the final amount of damage for the heaviest projectile thus compensating the non-linear effects.

ACKNOWLEDGEMENT

Work was supported by RFBR (Grant No. 10-08-91751) and Academy of Finland under the ENIGAZ project. Grants of computer time from the Center for Scientific Computing in Espoo, Finland, are gratefully acknowledged.

[1]Y. Ohki, Y. Toyoda, H. Kobayashi, and I. Akasaki, Inst. Phys. Conf. Ser. **63**, 479 (1982).
[2]E. Matioli, C. Neufeld, M. Iza, S. C. Cruz, A. A. Al-Heji, X. Chen, R. M. Farrell, S. Keller, S. DenBaars, U. Mishra, S. Nakamura, J. Speck, and C. Weisbuch, Appl. Phys. Lett. **98**, 021102 (2011).
[3]Y. Hao, L. Yang, and J. Zhang, Terahertz Sci. Technol. **1**, 51 (2008).

[4]V. D. S. Dhaka, N. V. Tkachenko, H. L. E.-M. Pavelescu, M. Guina, A. Tukiainen, J. Konttinen, M. Pessa, K. Arstila, J. Keinonen, and K. Nordlund, Semicond. Sci. Technol. **21**, 661 (2006).
[5]V. D. S. Dhaka, N. V. Tkachenko, H. L. E.-M. Pavelescu, S. Suomalainen, M. Pessa, K. Arstila, J. Keinonen, and K. Nordlund, J. Phys. D: Appl. Phys. **39**, 2659 (2006).
[6]C. Björkas, K. Nordlund, K. Arstila, J. Keinonen, V. D. S. Dhaka, and M. Pessa, J. Appl. Phys. **100**, 053516 (2006).
[7]A. I. Titov, S. O. Kucheyev, V. S. Belyakov, and A. Y. Azarov, J. Appl. Phys. **90**, 3867 (2001).
[8]A. I. Titov, P. A. Karaseov, A. Y. Azarov, and S. O. Kucheyev, Nucl. Instrum. Methods Phys. Res. B **267**, 2701 (2009).
[9]P. A. Karaseov, A. Y. Azarov, A. Titov, and S. Kucheyev, Semiconductors **43**, 691 (2009).
[10]S. O. Kucheyev, A. Y. Azarov, A. I. Titov, and P. Karaseov, J. Phys. D: Appl. Phys. **42**, 085309 (2009).
[11]S. Bouneau, A. Brunelle, S. Della-Negra, J. Depauw, D. Jacquet, Y. L. Beyec, M. Pautrat, M. Fallavier, J. C. Poizat, and H. H. Andersen, Phys. Rev. B **65**, 144106 (2002).
[12]J. Samela and K. Nordlund, Phys. Rev. B **76**, 125434 (2007).
[13]J. Nord, K. Albe, P. Erhart, and K. Nordlund, J. Phys.: Condens. Matter **15**, 5649 (2003).
[14]S. Saito, Y. Endo, and E. Hirota, J. Chem. Phys. **85**, 1778 (1986).
[15]G. S. Tschumper, J. T. Fermann, and H. F. Schaefer, J. Chem. Phys. **104**, 3676 (1996).
[16]F. M. Tao, J. Chem. Phys. **98**, 2481 (1993).
[17]J. F. Ziegler, J. P. Biersack, and U. Littmark, *The Stopping and Range of Ions in Matter* (Pergamon, New York, 1985).
[18]J. F. Ziegler, SRIM-2008.04 software package, available at http://www.srim.org.
[19]K. Nordlund, PARCAS computer code, 2010, The main principles of the molecular dynamics algorithms are presented in Refs. 21 and 24. The adaptive time step and electronic stopping algorithms are the same as in Ref. 25.
[20]H. J. C. Berendsen, J. P. M. Postma, W. F. van Gunsteren, A. DiNola, and J. R. Haak, J. Chem. Phys. **81**, 3684 (1984).
[21]K. Nordlund, M. Ghaly, R. S. Averback, M. Caturla, T. Diaz de la Rubia, and J. Tarus, Phys. Rev. B **57**, 7556 (1998).
[22]J. Nord, K. Nordlund, and J. Keinonen, Phys. Rev. B **68**, 184104 (2003).
[23]C. Björkas and K. Nordlund, Nucl. Instrum. Method Phys. Res. B **259**, 853 (2007).
[24]M. Ghaly, K. Nordlund, and R. S. Averback, Philos. Mag. A **79**, 795 (1999).
[25]K. Nordlund, Comput. Mater. Sci. **3**, 448 (1995).